A technique to increase the scanning rate of a phased array weather radar

V. M. Melnikov, R. J. Doviak, and D.S. Zrnic

University of Oklahoma, CIMMS and NOAA/OAR National Severe Storms Laboratory, Norman, Ok.

1. Introduction

Severe weather phenomena develop so fast that update time for radar remote sensing should be less than 1 min (e.g., [1]). The shortest update time for the current network of WSR-88D conventional radars is 4.5 min. The update time can be reduced with an agile-beam radar that steers its beam electronically (e.g., [2]). To reduce the update time on a prototype of a 10 cm wavelength phased array radar (PAR) located in Norman, OK, multiplexing of radar beams [3], oversampling and whitening in range [4], and adaptive scanning [5] have been tested. Multiplexing of radar beams aims at reducing correlation between weather signal (i.e., echoes) samples from different radar resolution volumes to reduce the standard deviations in estimated parameters for a given fixed number of collected samples, or at decreasing the number of samples required for spectral moment estimation to achieve a more rapid sampling of weather. Similarly, oversampling and whitening in range decorrelate return signals within the radar pulse which can be used to reduce the standard deviation of estimates, decrease dwell time, or a combination of both [4]. Aimed at increasing update rates of severe weather, adaptive scanning updates more frequently sections of the volume coverage pattern where weather returns are present and less frequently areas with no radar echoes [5].

Update times can also be reduced with frequency-agile radars and imaging radars. Frequency allocation at S band for weather radars is stringent. The frequency band for a network WSR-88D radar is 0.7 MHZ so no frequency agile technique is commonly implemented with the S-band weather radars; however, the frequency agile technique was used to shorten the update time for a 3 cm wavelength weather radar used for research [6]. Given the demands on spectral usage, it is unlikely bandwidth allocation will be increased. Thus, this technique is unlikely an option for the future weather PAR. To decrease update time, an imaging radar transmits a wide beam and forms multiple receiving beams of a phased array [7 – 11, 19, 20]. The major pitfall of this approach for weather applications is a reduced radiation power density of the transmit beam and consequently reduced detection capability. Detection capability attained with the WSR-88D has become a standard for operational weather radars in the US. It is evident that other alternatives should be explored, and one such alternative is described in this paper.

The update time of a PAR can be reduced by switching the beam directions of each of several pulses transmitted in rapid succession (e.g., pulse separations about a pulse width) so that multiple beams in transmit can be formed. Return signals from these beams can then be received simultaneously [12]. To isolate weather signals, phase coding for every transmit pulse could be employed. This technique is a particular implementation of the MIMO radars (Multiple In Multiple Out, e.g., [9]). Coding of transmitted pulses have also been considered to reduce coupling between received signals; the Walsh coding [13] or 13-bit Barker code have been studied [12]. Experiments using the Barker code showed a good spatial isolation for reflectivity fields having no strong gradients [12]. This technique is attractive but its implementation in the weather PAR is questionable because phase coding is used in the WSR-88D to resolve range ambiguities and most likely will be employed in the future weather PAR.

In this paper, we analyze a different technique to isolate returns from different directions using the multiple transmit beams technique. This technique does not use pulse coding. Section 2 describes the technique using the theoretical pattern of the WSR-88D in which sidelobes due to the feed support spars are ignored. In section 3, the technique is applied to data collected with a WSR-88D using a measured radiation pattern.

1. Description of the technique

a. WSR-88D KOUN's antenna pattern

Consider circular symmetric radiation described by the one-dimensional pattern function of the transmitted electric field given (in dB) by

$$G_1(\theta) = 20\log_{10}\left[g^{1/2} f(\theta)\right], \qquad (1)$$

where g is the one-way power density gain along the beam (i.e., mainlobe) axis and $f^2(\theta)$ is the normalized power density pattern $G_1(\theta)$ [14, section 3.1.2]. The zenith angle θ is measured from the beam axis (i.e., the polar axis). We focus on the transmitted electric field and received voltage patterns because weather signal voltages are used to suppress the ground clutter, resolve range foldings, and determine spectral moments and polarimetric parameters of precipitation, and thus we focus on retrieving voltages.

The antenna pattern of the legacy WSR-88D (i.e., one that transmitted and received only H polarized fields before changes were made to upgrade the WSR-88D radars to have H and V polarimetric measurement capability) measured by the manufacturer (i.e., Andrew Canada [15]) is summarized in Fig. 1 and compared with a theoretical pattern for KOUN, NSSL's Research and Development WSR-88D. Polarimetric upgrades should not change the pattern as is shown in an NSSL report [16]. The mainlobe measurements (circles in Fig. 1) were made on NSSL's "antenna range"; these data points are obtained from KOUN pattern measurements made after polarimetric upgrades by NSSL engineers for testing and evaluating the polarimetric capabilities before upgrades were made by the NWS to its network of WSR-88Ds.

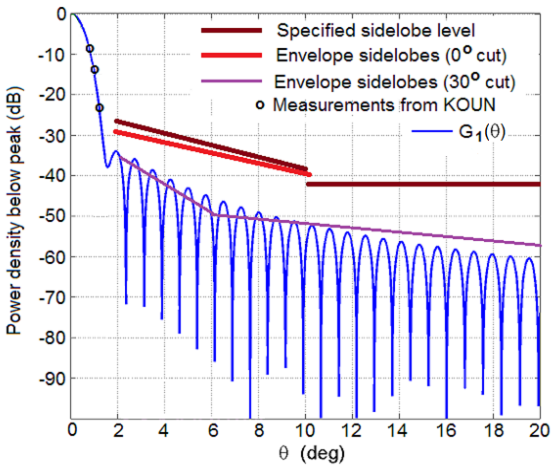

Fig. 1. The theoretical one-way power density pattern, $G_1(\theta)$, as a function of zenith angle θ for KOUN's antenna and comparison with measurements.

Sidelobe levels are represented by the envelope (magenta line) of the peak side lobes measured (without radome) for the 30° cut by Andrew Canada on its antenna range. The 30° cut avoids the ridge of high sidelobes due blockage from feed support spars and thus this pattern is representative of most of the volume illuminated by sidelobes and should also be one that is achievable with a weather PAR. Although this pattern was not measured for the KOUN antenna, this envelope should be representative of sidelobe levels along a 30° cut for any WSR-88D antenna (including the KOUN) assuming the WSR-88D radome does not significantly increase these very weak sidelobes. The 30° cut sidelobe level of the center-fed WSR-88D reflector is practically the same as that obtained for an offset-feed and reflector that has no beam blockage associated with feed support spars (e.g., compare Fig.1 with Fig.7 in [17]).

The red line is the envelope of KOUN sidelobes along a ridge of enhanced sidelobes due to feed support blockage caused by the vertical spar [16]. The KOUN sidelobes were measured by NSSL engineers after they converted KOUN to have dual polarimetric capability. These sidelobes include the effects of the radome and are less than a couple of dB larger than those 0° cut measurements made by Andrew Canada at their range using a WSR-88D reflector without a radome. Some of

the measured KOUN sidelobe level increase over that seen from Andrew Canada's data could be partly due to the radome, and partly due to artifacts (e.g. buildings, towers, etc.) on NSSL's antenna range. NSSL's antenna range is an ad hoc one in which homes and urban buildings densely populate the terrain between KOUN and a standard gain horn atop a 14 story building 3.4 km from KOUN. Such artifacts make it difficult to measure low level sidelobes. Although the ridge of sidelobes occupies a fraction of the entire radiation pattern, it is several dB larger than the sidelobe levels outside the ridge as seen in this figure. It is worth mentioning that this ridge of sidelobes has not been a detriment to the operation of the network of WSR-88Ds, nor for the interpretation of weather radar data.

b. Two transmitted pulses

Consider a phased array antenna consecutively transmitting RF pulses to two different directions. The time delay between these pulses is of the order of a pulse width τ. In reception, the PAR can synthesize weather signals from the array elements to construct receive beams simultaneously pointed in two different directions and weather signals from these receive beam directions can be simultaneously sampled and processed.

A radar receiver sets to sample voltage V(θ, r_n) from a resolution volume V_6 (θ, r_n) at direction θ with the center at distance of r_n. Assume the first pulse is transmitted principally along the direction $\theta = 0^o$ and the second pulse principally along the direction of γ degrees (because of sidelobes the pulses are transmitted in all directions although with considerably reduced power). For the 0^o and γ^o beams, the receiver simultaneously measures voltages not only from the directions of 0^o and γ^o (i.e., mainlobe-to-mainlobe coupling), but also along those sidelobes that coincide with the transmitted beam directions (i.e., mainlobe-to-sidelobe coupling). Placing the beams in the nulls of the sidelobes could minimize the mainlobe-to-sidelobe coupling factor, but herein for illustration we consider the γ^o beam location coinciding with the peak of the γ sidelobe of the 0^o beam.

Assume the sample spacing is equal to the pulse width. For weather radars having well-designed antennas (e.g., those used with the WSR-88D) and transmitting pulses in a single direction, sidelobe-to-sidelobe coupled power is negligible for most commonly observed circumstances. This is so because weather signals received via sidelobes are attenuated by the two-way (i.e., radiation/reception) pattern, and if one-way sidelobes levels are 50 dB below the mainlobe (e.g., Fig.1) the two-way radiation/reception pattern attenuates sidelobe coupled power by 100 dB. Associated with each weather signal sample for transmissions and reception along a single beam there is one corresponding resolution volume V_6 containing the scatterers that principally contribute to the sampled signal (herein this signal is associated with mainlobe-to-mainlobe coupling) . However, if pulses are sequentially transmitted along two beams, there are two additional V_6s contributing significant powers through sidelobes and these cannot be ignored if they are from a region where sidelobes intersect with the mainlobe (i.e., mainlobe-to-sidelobe coupled power).

To determine the V_6s containing scatterers contributing to the sampled weather signal, consider first the receiver R_0 associated with the 0^o receive beam and a gate that samples weather signals from V_6 (0^o, r_0). Although pulses are sequentially transmitted first on the 0^o beam and then on the γ^o beam, the resolution volume V_6 (0^o, r_0) is illuminated both by the 0^o transmit beam and as well the - γ^o sidelobe of the γ^o transmit beam. For weather signals received on the 0^o receive beam, the scatterers in V_6 (0^o, r_0) return weather signals due to usual mainlobe-to-mainlobe coupling (the blue sector in Fig. 2a). The yellow sector in Fig. 2a is V_6 that has sidelobe-to-sidelobe coupling for the transmitting and receiving beam at 0^o. Signal from this gate can be neglected. There are two V_6s that contribute mainlobe-to-sidelobe coupled weather signal components to the gate $R_0(0^o, r_0)$. For one the γ^o transmit beam has a sidelobe at -γ^o and so it also illuminates resolution volumes in the 0^odirection (the red sector in Fig. 2b). Because this sidelobe pulse is transmitted immediately after the 0^o beam pulse (i.e., with a delay τ), the sampling gate $R_0(0^o, r_0)$ also simultaneously samples these echoes, but they are associated with V_6 (0^o, r_{-1}). The second mainlobe-to-

sidelobe coupled weather signal sampled simultaneously by $R_0(0^o,r_0)$ emanates from$V_6(\gamma,r_{-1})$ (the green sector in Fig. 2b). This is the one received by the + γ^o sidelobe of 0^o receive beam when scatterers in this volume are illuminated by the γ^o transmit beam. Thus, there are three resolution volumes shown in Fig.2c that provide signals simultaneously sampled with the (0^o, r_0) gate.

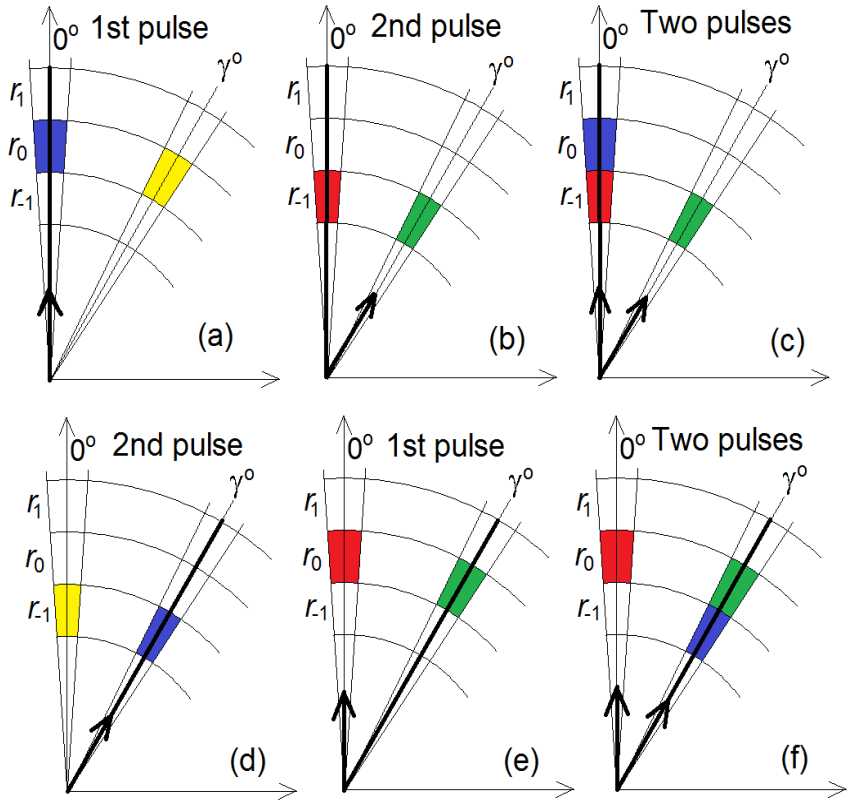

Fig.2. (a - c): Diagram showing resolution volumes V_6's (colored sectors) having scatterers that simultaneously contribute to a weather signal sampled with gate $R_0(0^o,r_0)$. The directions of transmitted pulses are shown with the thick black arrow. The receiving beam in 0^o direction is shown with the long thick black line. The blue range gates correspond to mainlobe-to-mainlobe coupling, the green and red ones correspond to mainlobe-to-sidelobe coupling, and the yellow gate is for sidelobe-to-sidelobe coupling. (d-f): Same as for (a-c) but for receiver $R_\gamma(\gamma,r_{-1})$, i.e., for γ^o direction.

Let $V(0^o, r_n)$ and $V(\gamma, r_n)$ be voltages received from 0^o and γ^o directions through the mainlobe-to-mainlobe coupling. These voltages have would be measured by radar in absence of mainlobe-to-sidelobe coupling. Obtain voltages that are received by receiver R_0 from the pulse transmitted in direction γ^o. One contribution (shown in Fig. 2b with red color) comes from $V_6(0^o, r_{-1})$ as being illuminated through the sidelobe at $-\gamma^o$ relative to the transmit direction. This contribution is $\beta(-\gamma)V(0^o,r_{-1})$, i.e. the true voltage attenuated by $\beta(-\gamma)$; this attenuation coefficient β is derived in the Appendix. The second contribution (shown in Fig. 2b with green) is received by R_0 from the second transmitted pulse from $V_6(\gamma, r_{-1})$ through the sidelobe. This contribution is $\beta(\gamma)V(\gamma,r_{-1})$. The measured voltage $U(0^o, r_0)$ received by R_0 from r_0 is the sum of the three voltages:

$$U(0^o,r_0) = V(0^o,r_0) + \beta(\gamma)V(\gamma,r_{-1}) + \beta(-\gamma)V(0^o,r_{-1}). \quad (2)$$

For mainlobe-to-mainlobe coupling, the echoes are weighted by the full gain of the 0^o beam, whereas mainlobe-to-sidelobe coupling, the echoes are weighted by the gain of the $-\gamma^o$ and γ^o sidelobes of the γ^o and 0^o beams, respectively.

It is seen from (2) that $U(0^o,r_0)$ depends upon $V(\gamma,r_{-1})$. Consider the receiver R_γ that samples weather signals on the γ degrees receive beam in which the $R_\gamma(\gamma, r_{-1})$ gate samples signals simultaneously with the $R_0(0^o, r_{-1})$ gate. As with signals sampled by the $R_0(0^o, r_0)$ gate, all weather signal components are sampled simultaneously but arrive from three different V_6s as shown in Figs.2f. Signal from the yellow sector in Fig. 2d has sidelobe-to-sidelobe coupling and thus is neglected. Because the pulse transmitted along the γ beam is delayed by τ, the mainlobe-to-mainlobe coupled signal on the γ^o receive beam is from $V_6(\gamma, r_{-1})$ (the blue sector in Fig. 2d). The other two resolution volumes produce sampled weather signals due to mainlobe-to-sidelobe coupling. The mainlobe-to-sidelobe coupled weather signal from $V_6(\gamma, r_0)$ is due to scatterers being illuminated by the +γ sidelobe of the 0^o transmit beam and received on the γ beam (the blue sector in Fig. 2e). The mainlobe-to-sidelobe coupled weather signal from $V_6(0^o, r_0)$ is due to scatterers being illuminated by the 0^o transmit beam and received on the $-\gamma$ sidelobe of the γ^o beam (the red sector in Fig. 2e). The measured voltage $U(\gamma,r_{-1})$ received by the receiver R_γ is the sum of the three voltages (Fig. 2f):

$$U(\gamma, r_{-1}) = V(\gamma,r_{-1}) + \beta(-\gamma)\, V(0^o,r_0) + \beta(\gamma)\, V(\gamma,r_0). \quad (3)$$

Voltage $U(\gamma,r_{-1})$ contains $V(\gamma,r_{-1})$ as a mainlobe-to-mainlobe contributor that enters in (2) as a mainlobe-to-sidelobe term. The third voltage on the right side of (2) can be obtained from a mainlobe-to-mainlobe contributor for voltage $U(0^o,r_{-1})$ which can be written using (2) as

$$U(0^o,r_{-1}) = V(0^o,r_{-1}) + \beta(\gamma)V(\gamma,r_{-2}) + \beta(-\gamma)V(0^o,r_{-2}), \quad (4)$$

Substitute $V(\gamma,r_{-1})$ from (3) and $V(0^o,r_{-1})$ from (4) into (2):

$$V(0^o,r_0) = U(0^o,r_0) - \beta(\gamma)U(\gamma,r_{-1}) - \beta(-\gamma)U(0^o,r_{-1}) +$$

$$\beta^2(\gamma)\, V(\gamma,r_0) + \beta(\gamma)\, \beta(-\gamma)[V(\gamma,r_{-2}) + V(0^o,r_0)] + \beta^2(-\gamma)\, V(0^o,r_{-2}). \quad (5)$$

Eq. (5) is convenient because it represents signals contributions as a power series of β. Since $\beta << 1$ this series converges fast. By using similar substitutions we can have a series with increasing powers of β and truncate the series to obtain a desired accuracy. Make the next step and express voltages V in (5) in terms of U using (2) and (3). We arrive to the following series:

$$V(0^o,r_0) = U(0^o,r_0) - \beta(\gamma)A_1 + \beta^2(\gamma)A_2 - \beta^3(\gamma)A_3 + \beta^4(\gamma)A_4 + o(\beta^5) \quad (6a)$$

with

$$A_1 = U(\gamma,r_{-1}) + U(0^o,r_{-1})\, \delta, \quad (6b)$$

$$A_2 = U(\gamma,r_0) + [U(0^o,r_0) + U(\gamma,r_{-2})]\delta + U(0^o,r_{-2})\, \delta^2, \quad (6c)$$

$$A_3 = U(\gamma,r_1) + U(0^o,r_1)\, \delta + U(\gamma,r_{-3})\, \delta^2 + U(0^o,r_{-3})\, \delta^3, \quad (6d)$$

$$A_4 = U(\gamma,r_2) + U(0^o,r_2)\, \delta + U(\gamma,r_{-4})\, \delta^3 + U(0^o,r_{-4})\, \delta^4, \quad (6e)$$

$$\delta = \beta(-\gamma)\beta^{-1}(\gamma).$$

In (6), we neglected β^2, $2\beta^2$, and $3\beta^2$ terms in comparison with 1. True voltage V in (6a) is expressed in terms of measured voltages U. This is the solution for the problem with accuracy of β^4 for the beam in 0^o direction. To obtain voltage from r_0 at 0^o direction, measured voltages from r_{-4} to r_2 for the two beams are used.

By omitting terms of β^5 magnitude, we obtain the solution with this accuracy, which does not modify weather echoes at a noticeable level. Eqs. (6a) and (7a) allow obtaining true voltages V from measured voltages U for the beams at 0^o and γ^o directions. Thus by injecting two pulses in two different directions and receiving signals from those two directions simultaneously, we obtain true voltages from the two directions via (6a) and (7a). So radar can scan two directions over time devoted for one pulse that equivalent to two times faster scanning. By transmitting three sequential pulses it is possible to triple the scanning rate. Corresponding equations can be derived in a way similar to one used to obtain (6a) and (7a).

The multiplexed beam technique (MBT) considered herein can be compared with the imaging radar concept where one wide transmit pulse is used to illuminate

large portion of clouds and multiple beams in receive are synthesized. The difference between these techniques is as follows. a) The imaging radar cannot achieve sensitivity of a single beam radar because transmitted power is injected into a very wide angle. The MBT has no degradation of sensitivity because all beams have the same power as the one in the single beam radar. b) The imaging radar illuminates a large cloud area so effects of sidelobes from all angles should be taken into consideration. In the MBT, few directions can be sampled simultaneously and effects of the sidelobes are eliminated by the restoration procedure eqs. (6-7).

c. Extreme cases

Weather observations with the WSR-88Ds are conducted with an accuracy imposed by the antenna sidelobes. The highest level of theoretical antenna pattern (Fig. 1) of the WSR-88Ds is -35 dB. The maximum sidelobe level of the two-way diagram is then -70 dB. This means that the radar receiver produces signal lower than noise if the main antenna lobe is directed in the clear sky and there is an object with signal-to-noise ratio (SNR) $\leq$ 70 dB in the direction of the highest sidelobe. All other sidelobes produce lower signals and these contributions are neglected. So the above technique with two transmit pulses must generate spurious signals below noise if SNR in the direction of the second pulse is of 70 dB and there is no echo in direction of the main lobe.

Solutions for true voltages (6a) and (7a) for two transmitted pulses are presented as a power series of $\beta(\gamma)$. Consider a case with SNR = 70 dB in direction of the second transmit pulse at 8.5°, for which $f^2(\gamma)$ = -50 dB (Fig. 1). Voltage $U(0^o,r_0)$ can be obtained from (2) with no signal in direction of the main lobe, i.e., $V(0^o,r_n) = 0$. Sidelobe-mainlobe leakage in this case is 70 -50 = 20 dB, which is very strong, and to eliminate this leakage, we have to apply the restoration procedure (6) and (7). By applying (7) with just three terms, i.e., with $\beta^2(\gamma)$ accuracy, we obtain the amplitude of $V(0^o,r_0)$ of equivalent power of -23 dB, which is below the noise level (0 dB). Thus despite the measured voltage $U(0^o,r_0)$ of 20 dB power, three-term (7a) delivers $V(0^o,r_0)$ with a negligible power as it should be because there is no echo in the main lobe. Three-term form of (7a) is sufficient because of β^2 is as low as -50 dB. For lower isolation, more terms in (7a) should be used to get correct voltages.

The antenna pattern of the dual-polarization WSR-88D is shown in Fig. 3. This radiation pattern was measured by Seavey Engineering at their antenna measurement facility after the installation of a dual polarimetric feed horn. Although there are both H and V patterns we focus our attention on the transmission and reception of horizontally polarized waves because the analysis of sidelobe coupled power presented herein applies either to the H or V. This is the pattern across a ridge of high sidelobes due to a vertical spar supporting the feed horn and thus it is not representative of the radiation pattern for most of the 2D angular space. Although this sidelobe pattern could have been corrupted by artifacts on the antenna range, it nevertheless can be used to simulate a worst case real sidelobe pattern along the azimuth direction and can be used to effectively simulate the mainlobe-to-sidelobe coupling for beams time multiplexed to different azimuthal directions.

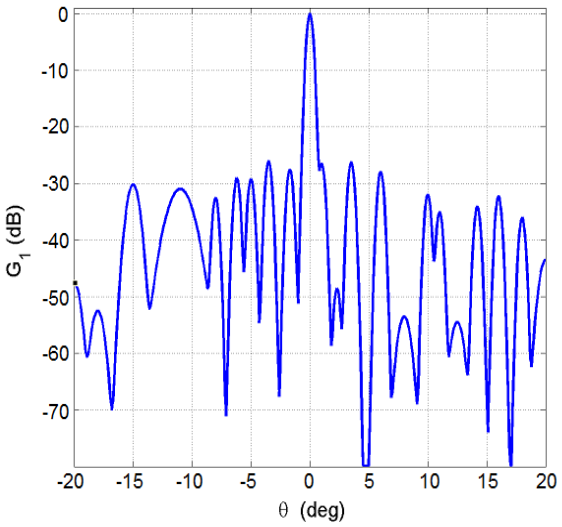

Fig.3. The WSR-88D's one-way radiation pattern of the dual polarization antenna at 2.7 GHz for horizontally polarized wave. This pattern is along the ridge of high sidelobes due to the feed support spars.

It is seen that there are angle intervals with sidelobe levels below -50 dB, e.g., θ = 7.5°, 12°, -18°. For the above two-pulse scheme, it is needed that product $f(\theta)$ $f(-\theta)$ be of -50 dB, which is not the case for the

indicated three angles because the diagram is not symmetrical. It is also desirable that the sidelobe in a direction of the second pulse has a form of a lobe but not a slope because a slope is more sensitive to non-uniformities in weather echoes than the lobe is. In addition to this, the antenna pattern of a weather PAR will be most likely worse than the pattern of a dish antenna.

Consider a dependence of the accuracy of (6a) and (7a) upon isolation $\beta(\gamma)$ for an antenna diagram with a symmetric angle intervals where $f(\gamma) = f(-\gamma)$. Directions 6^o and -6^o in Fig. 3 can be such directions with accuracy of 0.5 dB (the right lobe is a bit stronger than the left one). Let there be a strong reflecting core with SNR = 70 dB in the direction of main lobe (0^o) and no target present in direction γ^o. Fig. 4a presents the difference between the true and obtained SNR as a function of isolation β for five forms of (6a) with one, two, three, four and five power terms of β in its right hand part. The vertical axis in panel (a) presents the difference between calculated SNR and the true SNR of 70 dB. One can see that the difference is less than 0.2 dB at $\beta^2 < -20$ dB for just two-term form of (6a), i.e., $V(0^o,r_0) = U(0^o,r_0) - \beta(\gamma)A_1$ (the green curve).

Signal leakage into direction of γ is shown in Fig. 4b. No target is present in the direction and what is shown is the intensity of leakage. It is seen that the simplest form of (7a) (the blue curve) produces leakage of 30 dB at $\beta^2(\gamma) = -40$ dB of isolation. Noise level is shown in the panel with the dashed brown line. Four-term form of (7a) produces negligible leakage at $\beta^2 < -22$ dB (noise level of the light blue curve).

Signal leakage into direction of γ is shown in Fig. 4b. No target is present in the direction and what is shown is the intensity of leakage. It is seen that the simplest form of (7a) (the blue curve) produces leakage of 30 dB at $\beta^2(\gamma) = -40$ dB of isolation. Noise level is shown in the panel with the dashed brown line. Four-term form of (7a) produces negligible leakage at $\beta^2 < -22$ dB (noise level of the light blue curve).

Practically achievable leakage in a PAR antenna is about –25 dB so the four-term versions of (6a) and (7a) are sufficient in such a case with SNR as strong as 70 dB. It can be shown that at such isolation, the five-term form of (6a) and (7a) restores true voltages in both transmit directions at SNR difference of 93 dB in these directions. Thus isolation of -25 dB becomes equivalent to isolation of -46.5 dB if the restoration procedure (6) – (7) is applied.

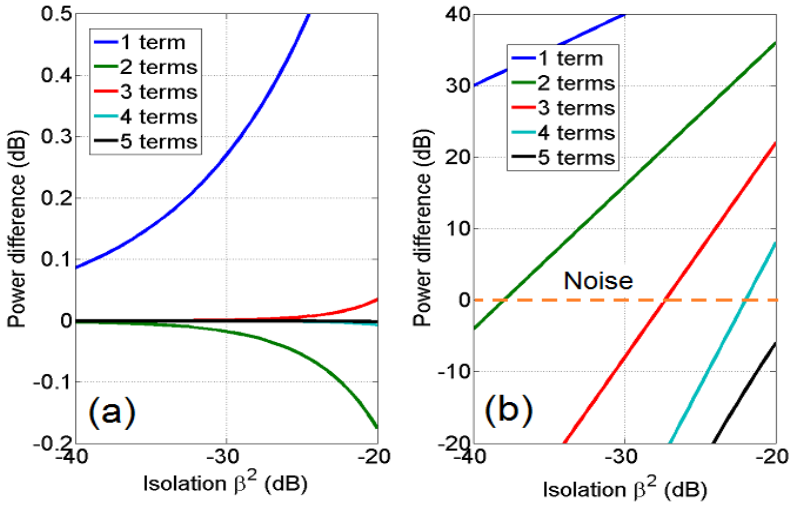

Fig. 4. (a) Difference in powers in the direction of main antenna lobe for SNR = 70 dB and various truncations of series (6a). (b) Same as in (a) but for the beam in direction with no reflecting object. The noise level is shown with the dashed brown line.

2. Using the WSR-88D's antenna pattern and data to show the effects of mainlobe–to-sidelobe coupling

Although the radiation pattern of a future weather PAR will be different from that for the present WSR-88Ds, it is of interest to assess effects of mainlobe-to-sidelobe coupling for time multiplexed transmissions using real storm data and the measured WSR-88D radiation pattern. This will be accomplished by simulating multiplexed transmissions and simultaneous reception using two beams and real storm data.

Consider time multiplexing of two pulses sequentially transmitted by a simulated PAR in the two azimuths φ = 0° and 6° and having the radiation patterns shown in Fig. 3: the first pulse is transmitted at 0° direction and the second pulse is transmitted at 6° direction. This direction is chosen because the width of the antenna lobe is very close to 1°, i.e., to the width of the mainlobe so that $\alpha = 1$ in (A8). At $\theta = 6°$, the value of $f^2(\theta)$ is -27.9 dB.

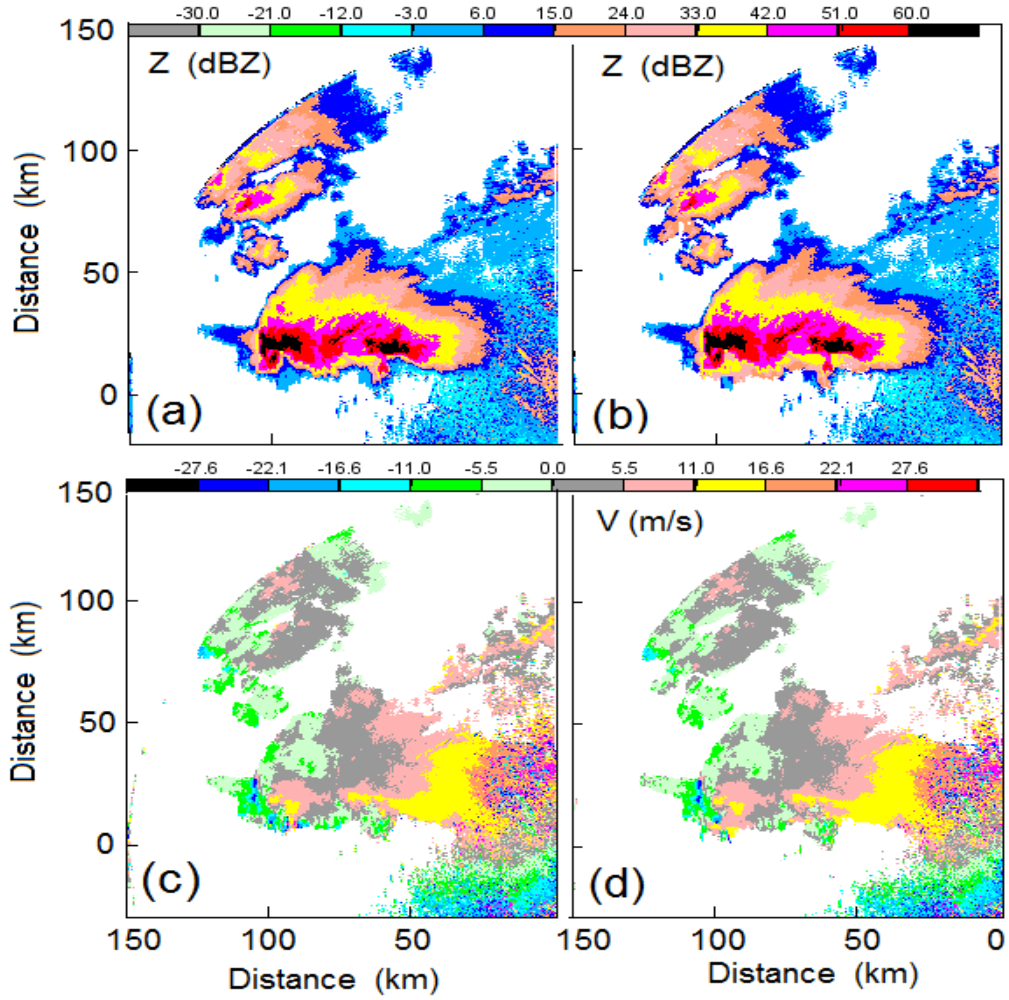

Fig. 5. (a): Reflectivity field collected with KOUN on March 31, 2008 at 0334Z at elevation of 1°. (b): Reflectivity field of the 0° beam showing contamination by mainlobe-to-sidelobe coupled power when using the 2-beam pattern. After applying the restoration procedure (6-7) the retrieved reflectivity field is exactly as shown in panel (a). Panels (c) and (d) are the same as (a) and (b) but present Doppler velocity.

To demonstrate effects of the sidelobes, time-series data collected with the WSR-88D KOUN were used. We take the KOUN data as "ground truth" and then emulate transmission of two beams at directions of 0^o and 6^o in azimuth off antenna boresite. All other sidelobes are not considered. This is made to show the effect of 6^o sidelobe. The time-series radar data are proportional to voltages of returned signals. Fig. 5a is assumed to represent the true reflectivity field and was obtained with KOUN on March 31, 2008 at 0334Z at elevation of 1^o. This is the field collected with a single radar beam and there is no mainlobe-to-sidelobe coupling. Figs. 5b,d present fields of reflectivity and Doppler velocities for the main lobe, i.e., U_0 with signal leakage from the beams that is described by eq. (2). Reflectivity field in Fig. 5a is for a tornadic thunderstorm with a hook echo located at the south-western part of the storm near the strongest reflectivity core. Despite rather coarse color gradations (6 dB) in the figure, one can see that the field in panel (b) has anomalous reflectivities in the weak reflectivity region of the hook echo to the south of the 60 dBZ reflectivity core. These anomalous reflectivities are due to the mainlobe-to-sidelobe coupling associated with product of the 6^o mainlobe gain. This exemplifies unacceptable mainlobe-to-sidelobe coupling. Despite the sidelobes of the two-beam pattern are weaker than -27.9 dB, the restoration procedure (6) – (7) is needed to get the undistorted field. After applying procedure (6) – (7) to the data in panel (b), a data field similar to panel (a) was restored.

Panels (c) and (d) demonstrate mainlobe-to-sidelobe signal leakage for the Doppler velocities. One can see that the field in the hook region gets severely distorted. All other estimates of weather variables (i.e., the spectrum width and polarimetric parameters) can be severely biased due to the sidelobes if the restoration procedure is not applied. Once the restoration procedure is applied, all fields become undistorted; the reflectivity field in Fig. 5(b) recovers to the one shown in Fig. 5(a). Thus, despite the weakness of the two-beam sidelobes, the restoration procedure (6-7) retrieves correct weather variables even in locations having strong reflectivity gradients.

3. Conclusions

The described multiplexed beam technique can reduce the update time by a number of times that equals to the number of beams transmitted by a PAR into different direction. The technique for two transmitted beams is considered above in detail. To separate the return signals, transmissions of pulses in directions of antenna sidelobes are used. No frequency agile and phase coding techniques to separate returns from different directions are used in the technique. The technique has the same sensitivity as usual single beam weather radars.

The technique allows separating of signal voltages; it should be applied first to separate signal returns from different directions. After that, known methods of signal processing can be applied. Thus all existing signal processing techniques in the WSR-88Ds weather radars that are in use to resolve range ambiguities and suppress ground clutter can remain the same. The only limitation for the technique is the duty cycle of the transmitter. The duty cycle must allow transmitting few pulses with small delays (order of microseconds). Data from distances close to the radar are lost due to transmission of radar pulses. For instance, if four 1.5 μs pulses can be transmitted with time delay of 1 μs between them, then the time for transmission is 4x1.5 μs + 3x1 μs = 9 μs that equals to 2.7 km of the lost distance, which is tolerable because data from first 5 km are strongly contaminated by ground clutter and typically are not used in S-band weather radars.

Practically achievable antenna sidelobes level in a PAR is about –25 dB. At such level, the five-term form of the technique [eqs. (6a) and (7a)] restores true voltages in both transmit directions at SNR difference of 93 dB in these directions, which means that antenna isolation of -25 dB becomes equivalent to isolation of -46.5 dB after the application of the technique. The technique has been demonstrated using weather data collected with the WSR-88D (Fig. 5); PAR operations have been applied in quasi-real time transmission of radar pulses. The proposed technique can be used in existing and future weather PARs, which are capable of transmitting radar pulses with a delay of a few microseconds.

Appendix. The attenuation coefficient for mainlobe-to-sidelobe coupling.

To derive the coefficient, consider first the power received from a range gate at distance r_0 at time t:(Doviak and Zrnic 2006, 4.4)

$$P(r_0,t) = C\eta(r_0,t)\int_0^{\pi} f^4(\theta)\sin\theta\, d\theta, \qquad \text{(A1)}$$

where $\eta(r_0,t)$ is instantaneous reflectivity, C depends on r_0 and radar parameters. Integration in (A1) is usually performed over the mainlobe of antenna radiation pattern that allows expressing the integral in terms of the radiation diagram width $\theta_1(0^o)$ in direction of 0^o (Doviak and Zrnic 2006, eq 4.13):

$$\int_0^{\pi} f^4(\theta - 0^o)\sin\theta\, d\theta = \theta_1^2(0^o)/16\ln 2. \qquad \text{(A2)}$$

Eqs (A1) and (A2) are written for the energy transmitted and received through the main antenna lobe. This is called herein mainlobe-to-mainlobe coupling. Consider a PAR radar that transmits a pulse to direction of 0^o and then immediately switches its receiving beam to direction of γ^o, i.e., consider receiver R_γ alone. The receiving beam samples signal from V_6 at r_0 which results from transmitted pulse trough a sidelobe at γ^o from 0^o direction and received by the mainlobe directed to γ^o. The received power can be written as

$$P(\gamma,r_0) = C\eta(\gamma,r_0)\int_0^{\pi} f_t^2(\theta-\gamma) f_r^2(\theta-0^o)\sin\theta\, d\theta. \qquad \text{(A3)}$$

Argument γ is introduced here to distinguish between the directions of transmission and reception; subscript t and r stand for transmission and reception. The behavior of $f(\theta - \gamma)$ around γ in (A3) can be obtained from function $f^2(\theta - \gamma)/ f^2(\gamma)$. Integration of the latter function over the main part of sidelobe leads to the width $\theta_1(\gamma)$ so that (A3) can be represented as

$$P(\gamma,r_0) = C_1\eta(\gamma,r_0) f^2(\gamma)\ \alpha(\gamma)\ \theta_1(0^o)\ \theta_1(\gamma), \qquad \text{(A4)}$$

with

$$\alpha(\gamma) = \frac{1}{f^2(\gamma)\theta_1(0^o)\theta_1(\gamma)}\int_0^{\pi} f^2(\theta-\gamma) f^2(\theta-0^o)\sin\theta\, d\theta \qquad \text{(A5)}$$

and $C_1 = C/16\ln 2$. In (A5) we assume that the diagram in transmit and receive are equal. It is convenient to present the power in form (A4) because it shows that this mainlobe-to-sidelobe coupling is $f^2(\gamma)$ times smaller than mainlobe-to-mainlobe term because $\theta_1(0^o)$ and $\theta_1(\gamma)$ are of the same order of magnitude and $\alpha \approx 1$; for $\theta_1(0^o) = \theta_1(\gamma)$, $\alpha = 1$. An equation similar to (A4) holds for case when PAR transmits a pulse into direction γ^o and then immediately switches to direction 0^o for reception. In this case, (A4) holds with γ replaced with $-\gamma^o$.

Transmission of two pulses into different direction is considered in section 2 and this requires introducing voltages that are proportional to the amplitude of an electromagnetic wave at the radar antenna. The amplitudes get added at the radar input so that voltages should be summed up. The instant received power is just

$$P(\theta,r_0) = V(\theta,r_0)\, V^*(\theta,r_0), \qquad \text{(A6)}$$

where the asterisk stands for complex conjugate. Voltages change in time because instant reflectivities change over time. Eq. (A4) is represented as

$$P(\gamma,r_0) = |V(\gamma,r_0)|^2\ f^2(\gamma)\ \alpha(\gamma)\ . \qquad \text{(A7)}$$

Here voltage $V(\gamma, r_0)$ is the one that can be received in mainlobe-to-mainlobe coupling with the beam directed in γ. Eq. (A7) has a simple meaning: when radar transmits its pulse in direction of 0^o and then switches its receive beam to γ, it receives voltage that is $f(\gamma)\ \alpha^{1/2}(\gamma)$ times smaller than it is in case when radar transmits and receives signals at direction γ.

Sidelobe-to-sidelobe coupling is neglected in the WSR-88Ds operations. This coupling for direction γ can be represented by the following voltage

$$V_s(\gamma,r_0) = V(\gamma,r_0) f^2(\gamma)\ \alpha^{1/2}(\gamma) = V(\gamma,r_0)\beta(\gamma) \qquad \text{(A8)}$$

with $\beta(\gamma) = f^2(\gamma)\ \alpha(\gamma)$, where subscript s stands for this type of coupling. One can see that multiplier $\beta(\gamma)$

attenuates true voltage for direction γ and this attenuation is strong because $f^2(\gamma) << 1$. Neglecting sidelobe-to-sidelobe coupling means neglecting voltages that have $f^2(\gamma)$ multiplier, i.e., we neglect power contributions of $f^4(\gamma)$ order.

To get sense of the strength of sidelobe-to-sidelobe coupling, consider the following example. The maximum measured sidelobe envelope of the WSR-88D is -30 dB (the red line in Fig. 1 at $\theta = 2^o$). Signals with signal-to-noise ratio (SNR) less than 2dB are considered as nonsignificant and are filtered out by the system. So the power that is suppressed by one-way sidelobes of -30 dB and creates SNR = 2 dB is 2*30 + 2 = 62 dB. For sidelobes at angles larger than 10^o, the envelope is about -40 dB (Fig. 1) and minimum tolerable SNR for signals from these sidelobes is 82 dB. The dynamic range of the WSR-88D receiver is about 95 dB, i.e., larger than 82 dB estimated for sidelobe-to-sidelobe coupling. So contaminations from the sidelobes should be visible in the WSR-88Ds and this indeed is observed.

Acknowledgment. We thank Mr. David Warde for the discussions.

References

[1] P.L. Heinselman, D. L. Priegnitz, K. L. Manross, T.M. Smith, R. W. Adams, 2008: Rapid Sampling of Severe Storms by the National Weather Radar Testbed Phased Array Radar. *Wea. Forecasting*, **23**, 808–824.

[2] D.S. Zrnic, J. F. Kimpel, D. E. Forsyth, A. Shapiro, G. Crain, R. Ferek, J. Heimmer, W. Benner, T. J. McNellis, R. J. Vogt: Agile-Beam Phased Array Radar for Weather Observations. *Bull. Amer. Meteor. Soc.*, **88**, 1753–1766.

[3] T-Y. Yu, M. B. Orescanin, C. D. Curtis, D. S. Zrnić, D. E. Forsyth, 2007: Beam Multiplexing Using the Phased-Array Weather Radar. *J. Atmos. Oceanic Technol.*, **24**, 616–626.

[4] S. Torres, and D. S. Zrnic, 2003: Whitening in range to improve weather radar spectral moment estimates. Part I: Formulation and simulation. *J. Atmos. Oceanic Technol.,* **20,** 1433–1448.

[5] R. Reinoso-Rondinel, S. Torres, T-Y. Yu, 2010: Task prioritization on phased-array radar scheduler for adaptive weather sensing. 26th Conference on Interactive Information and Processing Systems (IIPS) for Meteorology, Oceanography, and Hydrology. 14B.6.

[6] A.L. Pazmany, J. B. Mead, H. B. Bluestein, J. C. Snyder, J. B. Houser, 2013: A mobile rapid-scanning X-band polarimetric (RaXPol) Doppler radar system. *J. Atmos. Oceanic Technol.*, **30**, 1398–1413.

[7] R.D. Palmer, S. Gopalam, T.-Y. Yu, and S. Fukao, 1998: Coherent Radar Imaging Using Capon's Method. *Radio Sci*., **33**, 1585–1598.

[8] R.D. Palmer, B. L. Cheong, M. W. Hoffman, S. J. Frasier, and F. J. Lopez-Dekker, 2005: Observations of the Small-Scale Variability of Precipitation Using an Imaging Radar. *J. Atmos. Oceanic Technol.,* **22**, 1122–1137.

[9] J. Li, and P. Stoica, 2007: MIMO radar with collocated antennas. *IEEE Signal Proc. Magazine*, September, 106-114.

[10] C.C. Kidder, M. B. Yeary, R.D. Palmer, 2011: Beyond phased arrays – design principles for an imagine radar. IEEE RadCon conference.

[11] B. Isom, R. Palmer, R. Kelley, J. Meier, D. Bodine, M. Yeary, 2013: The atmospheric imaging radar: Simultaneous volumetric observations using a phased array weather radar. *J. Atmos. Oceanic Technol.*, **30**, 655–675.

[12] K.H. Lai, I.D. Longstaff, and G.D. Callahan, 2004: Super-fast scanning technique for phased array weather radar application. *IEEE Proc.: Radar Sonar Navig*., **151**, 271-279.

[13] H. Urkowitz, 1997: Reduction of sidelobe self-interference in agile beam multiplexing. IEEE National Radar Conf., Syracuse, NY, May 1997, 355-360.

[14] R.J. Doviak, and D. S. Zrnic, 2006: *Doppler radar and weather observations*, 2nd ed., Academic Press, 562 pp.

[15] Paramax, 1992: Test Report, Antenna/Pedestal, Part 1 of 4, Linear Polarized Antenna First Article, Document #: TR1218305, prepared for :U.S. Department of Commerce, Office of Procurement, Washington, DC 20230.

[16] R.J. Doviak, D. S. Zrnic, J. Carter, A. Ryzhkov, S. Torres, and A. Zahrai, 1998: Polarimetric upgrades to improve rainfall measurements. An NSSL report, April, 113 pp.

[17] V.N Bringi, R. Hoferer, D. A. Brunkow, R. Schwerdtfeger, V. Chandrasekar, S. A. Rutledge, J. George, P. C. Kennedy, 2011: Design and performance characteristics of the new 8.5-m dual-offset Gregorian antenna for the CSU–CHILL radar. *J. Atmos. Oceanic Technol.*, **28**, 907–920.

[18] H.E. Schrank, 1988: Low-sidelobe phased array and reflector antennas. Chapter 6 in *Aspects of Modern Radar*, E. Brookner Ed., Artech House, Boston, 574 pp.

[19] J.B. Mead, G. Hopcraft, S. J. Frasier, B. D. Pollard, C. D. Cherry, and D. H. Schaubert, 1998: A Volume-Imaging Radar Wind Profiler for Atmospheric Boundary Layer Turbulence Studies. *J. Atmos. Oceanic Technol.*, **15**, 849–859.

[20] D.L. Hysell, and R. F. Woodman, 1997: Imaging Coherent Backscatter Radar Observations
of Topside Equatorial Spread F. *Radio Sci.*, **32**, 2309–2320.